Chemical Engineering Journal 421 (2021) 129694

Contents lists available at ScienceDirect

Chemical Engineering Journal

journal homepage: www.elsevier.com/locate/cej

MP-PIC simulation of the effects of spent catalyst distribution and horizontal baffle in an industrial FCC regenerator. Part II: Effects on regenerator performance

Zhijun Yang [a,b], Yongmin Zhang [a,*], Tiebin Liu [b], Adefarati Oloruntoba [a]

[a] State Key Laboratory of Heavy Oil Processing, China University of Petroleum, Beijing 102249, China
[b] Dalian Research Institute of Petroleum and Petrochemicals, SINOPEC, Dalian 116045, China

ARTICLE INFO

Keywords:
FCC regenerator
Spent catalyst distribution
Horizontal baffle
MP-PIC simulation
Coke burning reaction
Afterburn

ABSTRACT

Improving distribution uniformity of spent catalyst and adding horizontal baffles are two effective measures to improve the regeneration performance of a fluid catalytic cracking (FCC) unit. In this study, the effects of the spent catalyst distribution and horizontal baffle on the regeneration performance of an industrial coaxial compact FCC regenerator is simulated using an Eulerian-Lagrangian multi-phase particle in cell (MP-PIC) method with coupled hydrodynamic and coke-burning kinetics models. The coke-burning kinetics model developed by Arbel et al. (Ind Eng Chem Res, 1995, 34(4): 1228–1243) is used in the simulation. The MP-PIC simulations successfully predicted agreeable temperatures in the industrial regenerator. Serious afterburning in the freeboard was also successfully predicted. The effectiveness of the two intensification measures in enhancing the performance of an industrial FCC regenerator were proved, as indicated by the restrained afterburning in the freeboard, the increased coke burning efficiency, the lower coke content in the regenerated catalysts. Comparatively, adding a properly design horizontal baffle was proved to be more effective and should be a primary intensification measure used in industrial regenerators. A better spent catalyst distributor was suggested to be used to help the inserted horizontal baffles further improve the performance of the regenerator. By the simulation, more flow-reaction coupling mechanisms during the regeneration process are capable to be understood in more depth. The effectiveness of different intensification measures depends both on the resulted matching quality between the distributions of spent catalyst and oxygen in the main air, and the solids residence time distribution.

1. Introduction

A regenerator is an essential component of an FCC unit, which is used to burn off the coke deposited on spent catalysts, restore their activity and then provide the required heat for the endothermic cracking reactions in a riser reactor [1]. The performance of a regenerator often determines the energy consumption cost and turnaround length of an FCC unit, and also affects the product yields indirectly and the unit profitability. For some old FCC units or some wanting to expand their processing capacities, the coke-burning capacity of their regenerator is often one of the main bottlenecking factors that need to be revamped and improved [2]. Moreover, afterburning (fast burning of CO in the freeboard resulting in excessive temperature) is another problem bothering many industrial FCC regenerators. Mostly, afterburning grows out of uneven contact between the coke in catalysts and the oxygen in the main air in the dense bed. Serious afterburning can result in damages of internal components (e.g. cyclone and outlet ducts), and unscheduled shutdown of the unit [3,4]. There are also other problems in an FCC regenerator, e.g. high air consumption, catalyst cooling bottleneck, serious operating instability, that limit the operation stability and profitability of an FCC unit.

In order to improve the performance and eliminate the above problems, a lot of regenerator optimization research efforts have been reported [5–8]. Improving spent catalyst distribution and adding horizontal baffles in the dense bed in a single-stage regenerator are often believed to be two economical and effective measures. KBR has proposed the RegenMax™ technology [9], which is to realize a two-stage countercurrent regeneration by adding a layer of corrugated packing internals in the dense bed of a single-stage regenerator. The RegenMax™ also emphasizes the importance of spent catalyst distribution uniformity. They have used an example [10] to demonstrate the advantage of

* Corresponding author.
E-mail address: zhym@cup.edu.cn (Y. Zhang).

https://doi.org/10.1016/j.cej.2021.129694
Received 21 January 2021; Received in revised form 28 March 2021; Accepted 1 April 2021
Available online 15 April 2021

Nomenclature

C_{rgc}	mass of coke on regenerated catalyst (kg)
H_{rgc}	mass of hydrogen on regenerated catalyst (kg)
C_p	mixture specific heat at constant pressure (J/mol·K)
$C_{p,i}$	specific heat of species *i* (J/mol·K)
C_v	specific heat of particle (J/kg·K)
d_p	individual particle diameter (m)
D	turbulent mass diffusivity
E_β	activation energy (J/mol)
h_g	gas enthalpy (J/mol)
$h_{g,i}$	enthalpy of gas species *i* (J/mol)
h_p	particle enthalpy (J/mol)
k_c	overall coke-burning rate coefficient
Mw_C	molecular weight of coke (kg/kmol)
Mw_H	molecular weight of hydrogen (kg/kmol)
Mw_i	molecular weight of gas species *i* (kg/kmol)
m_p	particle mass (kg)
$Nu_{g,p}$	Nusselt number for heat transfer in the gas to the particle
p	gas pressure (Pa)
Pr	Prandtl number
Pr_t	turbulent Prandtl number
q	gas heat flux (J/m^2)
$\dot{q}_D$	enthalpy diffusion term
$\dot{Q}$	energy source per volume (J/m^3)
R	universal gas constant (J/mol·K)
Sc	Schmidt number
S_h	conservative energy exchange from particle phase to gas phase (J/m^3)
t	time (s)
T_g	gas mixture temperature (K)
T_p	particle temperature (K)
T_{ref}	reference temperature (K)
$\vec{u}_g$	gas velocity (m/s)
$\vec{u}_p$	particle velocity (m/s)
$Y_{g,i}$	mass fraction of gas species *i*

Greek letters

θ_g	gas volume fraction
Φ	viscous dissipation
λ_g	gas thermal conductivity (W/m·K)
ρ_c	density of coke on catalyst (kg/m^3)
ρ_g	gas density (kg/m^3)
ρ_H	density of hydrogen on catalyst (kg/m^3)
ρ_p	particle density (kg/m^3)
μ_g	gas viscosity (Pa/s)
β_c	initial ratio of CO/ CO_2 at the catalyst surface
β_{c0}	pre-exponential constant
ε	small number with the order of 10^{-7}
$\delta\dot{m}_{i,chem}$	chemical source term for species *i*

this technology according to the regenerator model of Sapre et al. [11]. Using a feedstock with carbon residue of 5 wt%, they compared the different design and performances between a traditional full-burn single-stage regenerator and another partial-burn regenerator revamped according to RegenMax™ technology. A same requirement on carbon content in regenerated catalyst, i.e. 0.05 wt% applied to the two cases. Their estimation indicated that, [10] the new RegenMax™ regenerator decreases by 11% in diameter, 22% in air consumption, 5% in catalyst inventory and 10% in fresh catalyst supplement. Moreover, the catalyst cooler is no longer needed.

Although the RegenMax™ technology has been reported for many years, it has not been successfully implemented in industrial installations. Our research group [12] developed a new horizontal baffle called Crosser grid used to strengthen gas-solids contact and suppress gas/solids backmixing in fluidized bed reactors. Our mathematical baffled regenerator model [13] demonstrated that the regenerator with a layer of Crosser grid can achieve same regenerator performance with significantly reduced air consumption and catalyst inventory. The results of its industrial applications in FCC regenerators [14–16] showed that, after adding the Crosser grid in the regenerators, the lateral temperature difference in the dense bed decreases, afterburning in the freeboard is restrained remarkably which leads to less CO promoter usage, air consumption is decreased, and sometimes carbon content in regenerated catalyst is reduced.

Due to the huge volume, complex internal structure and high reaction temperature of industrial regenerators, it is difficult to investigate the complex coupled multiphase reactive flow by laboratory experiment. In recent years, with the rapid development of technologies in computer hardware and computational flow dynamics (CFD) algorithms, CFD simulation has been gradually accepted to investigate complex multiphase flow systems [17–20]. Up to now, only a few CFD simulation studies on industrial regenerators have been reported [21–23].

Tang et al. [24] is one of the few teams who have coupled hydrodynamics and coke-burning kinetics in their simulations of industrial FCC regenerators. In their study, they established a three-dimensional CFD model with multiple phases and species to simulate the hydrodynamics and reactions in an industrial FCC regenerator. Their simulation results showed the effect of oxygen enrichment on catalyst regeneration. They found that the coke-burning rate increased 90 ~ 94.5%, when the oxygen enrichment was 5%. However, as oxygen enrichment exceeded 5%, the effect on improving regeneration efficiency was not distinct any more.

Chang et al. [25] used a TFM model to simulate an industrial turbulent FCC regenerator where the influences of operating parameters on hydrodynamics and coke-burning reactions were both studied. The results showed that increasing superficial gas velocity and operating pressure could increase the coke-burning rate. However, increasing the initial coke content in spent catalyst and the circulation rate of spent catalyst would worsen the regenerator performance, especially leading to higher average carbon contents in both catalyst in bed and in regenerated catalyst.

Singh et al. [26] also conducted a simulation study on an industrial FCC regenerator using a MP-PIC model to quantitatively predict the profiles of bed density, temperature and the concentration of flue gas components in the regenerator. One of the key findings in their simulation is that the temperature difference between the dense bed and freeboard is very large, which demonstrates that the afterburning in the freeboard is very severe. To solve this problem, they proposed that improving the gas distributor layout could be a potential solution. The simulation results with an optimized gas distributor showed that the axial and lateral temperature distributions were more uniform and the afterburning was restrained.

Berrouk et al. [27] also used a MP-PIC model to conduct a simulation on an industrial FCC regenerator. The objectives of their study were to reveal the linkage between the performance and reliability problems in a regenerator and the structural designs of its internal components, i.e. air distributor, standpipe drainage and spent catalyst distributor, as well as the operating parameters. With the help of simulations, more constructive suggestions are expected to be proposed to guide future revamps to solve these problems.

Despite both hydrodynamics and coke-burning kinetics were

considered in the above studies on FCC regenerator, to our knowledge, simulation study on the effect of internal baffles and spent catalyst distribution on FCC regenerator performance, especially large-scale industrial FCC regenerators, has not been reported. Although mathematical regenerator models, e.g. in Sapre et al. [11] and Zhang & Lu [13], have been used to model industrial FCC regenerators and quantitative predictions on the regenerator performance parameters can be obtained. Too many simplifications were made in these models. The industrial community is difficult to trust these predicted results with high confidence. Moreover, detailed descriptions of the distributions of solids, temperature, coke content, flue gas compositions in the full three-dimensional space of an industrial FCC regenerator cannot be obtained by these modeling efforts.

Following a previous published paper which discussed the effects of spent catalyst distribution and horizontal baffle on the hydrodynamics of an industrial coaxial counter-current FCC regenerator [28], this paper, intends to present the effects of spent catalyst distribution and horizontal baffle on the regenerator performance using a same MP-PIC simulation method. First, the temperature distribution of four regenerators with different combination of spent catalyst distribution uniformity and with or without Crosser grid will be obtained. The effects of spent catalyst distribution uniformity and Crosser grid on the afterburning in the freeboard are also discussed. Second, the variations of flue gas component in the four different regenerators with time are obtained. The distribution of CO and O_2 in the regenerator, results of air distributor and spent catalyst distributor, are discussed to reveal the importance of uniform distribution of spent catalyst and air. Finally, the change in the carbon content in regenerated catalyst with time, the carbon content profile in the regenerator, and the residence time distribution and carbon content distribution of the regenerated catalysts are obtained to illustrate the influences of spent catalyst distribution uniformity and horizontal baffle on the coke-burning rate and the clearance of regenerated catalyst. It should be noted that all results in the two sequential papers were from a same series of MP-PIC simulations.

2. Model and simulation setup

The governing equations and drag model of the MP-PIC model have been given in Yang et al. [28]. The gas species transport equations, the energy conservation equations and kinetics model of coke-burning reaction are given below.

2.1. Gas species transport equations

The transport equation is employed for each gas species to describe the gas phase. The total gas phase properties are calculated from the mass fractions, $Y_{g,i}$, of the gas species. In the process of chemical reactions, mass is transferred between the gas species and is considered through the chemical source terms $\delta\dot{m}_{i,chem}$ in the individual gas species transport equation, as shown below:

$$\frac{\partial(\theta_g\rho_g Y_{g,i})}{\partial t}+\nabla\cdot\left(\theta_g\rho_g Y_{g,i}\vec{u}_g\right)=\nabla\cdot\left(\theta_g D\rho_g\nabla Y_{g,i}\right)+\delta\dot{m}_{i,chem} \quad (1)$$

where θ_g is the gas volume fraction, $\vec{u}_g$ is the gas velocity, ρ_g is the gas density, D is the intrinsic mass diffusivity and is related to the gas viscosity μ_g by the Schmidt number Sc, as given below:

$$Sc=\frac{\mu_g}{\rho_g D} \quad (2)$$

where $Sc = 0.9$ which is the default value.

2.2. Energy conservation equations

The energy conservation equation of gas phase is from the report of O'Rourke [29], as shown below,

$$\frac{\partial(\theta_g\rho_g h_g)}{\partial t}+\nabla\cdot\left(\theta_g\rho_g h_g\vec{u}_g\right)=\theta_g\left(\frac{\partial p}{\partial t}+\vec{u}_g\cdot\nabla p\right)+\Phi-\nabla\cdot\left(\theta_g q\right)+\dot{Q}+S_h+\dot{q}_D \quad (3)$$

Herein, h_g is the gas enthalpy, Φ is the viscous dissipation and $\dot{Q}$ is the energy source per volume. According to Snider et al. [30], disregarding the viscous dissipation implies that there is no energy source. The S_h denotes the conservative energy exchange from the particle phase to the gas phase, and q is the gas heat flux, as shown below,

$$q=-\lambda_g\nabla T_g \quad (4)$$

Herein, λ_g is the gas thermal conductivity which denotes the summation of a molecular conductivity and an eddy-conductivity from Reynolds stress mixing. The eddy-conductivity is obtained through a turbulent Prandtl number and is expressed as follows,

$$Pr_t=\frac{C_p\mu_t}{\lambda_t} \quad (5)$$

where Pr_t is a default value of 0.9.

The enthalpy diffusion term $\dot{q}_D$ in Eq. (3) is expressed as:

$$\dot{q}_D=\sum_{i=1}^{N_s}\nabla\cdot(h_{g,i}\theta_g\rho_g D\nabla Y_{g,i}) \quad (6)$$

where N_s is the summation of all gas species, and $h_{g,i}$ is the enthalpy of gas-phase species i.

Through the state equations, the pressure, enthalpy, temperature, density, and mass fractions of the gas phase are closely related. In the MP-PIC model, the partial pressure of gas species is calculated by the ideal gas state equation, as given below,

$$P_i=\frac{\rho_g Y_{g,i}RT_g}{Mw_i} \quad (7)$$

Herein, R is the universal gas constant, T_g is the gas mixture temperature, Mw_i is the molecular weight of gas species i. The relationship between gas thermodynamics pressure of the total mean flow and the species pressure is shown below,

$$P=\sum_{i=1}^{N_s}P_i \quad (8)$$

The mixture enthalpy is related to the species enthalpies, as shown below,

$$h_g=\sum_{i=1}^{N_s}Y_{g,i}h_{g,i} \quad (9)$$

The term C_p in Eq. (5) is the mixture specific heat at constant pressure and given by

$$C_p=\sum_{i=1}^{N_s}Y_{g,i}C_{p,i} \quad (10)$$

where $C_{p,i}$ is the specific heat of species i. The species enthalpies $h_{g,i}$ is a function of the gas temperature T_g , as given below,

$$h_{g,i}=\int_{T_{ref}}^{T_g}C_{p,i}dT+\Delta h_{g,i} \quad (11)$$

where $\Delta h_{g,i}$ is the heat formation of species i at the reference temperature T_{ref}.

With respect to the particle energy conservation equation, isothermal condition is assumed across the whole particle, implying that during the chemical reactions no heat is released within the particle. More so, during the chemical reactions, the heat liberated taking place on the particles' surfaces is directly associated with the gas-phase

energy, having no effect on the surface energy balance. Therefore, the lumped particle heat equation is as shown below,

$$C_v\frac{dT_p}{dt}=\frac{1}{m_p}\frac{\lambda_g Nu_{g,p}}{2r_p}A_p(T_g-T_p) \tag{12}$$

Herein, T_p is the particle temperature, C_v is the specific heat of particle, $Nu_{g,p}$ is the Nusselt number for heat transfer from the gas to the particle, andλ_g is the gas thermal conductivity.

The energy exchange from the particle phase to the gas phase is given below,

$$S_h=\iiint f\left\{m_p\left[D_p(\vec{u}_p-\vec{u}_g)^2-C_v\frac{dT_p}{dt}\right]-\frac{dm_p}{dt}\left[h_p+\frac{1}{2}(\vec{u}_p-\vec{u}_g)^2\right]\right\}dm_p d\vec{u}_p dT_p \tag{13}$$

where h_p is the particle enthalpy and expressed as

$$h_p=(2.0+1.2Re^{0.5}Pr^{0.33})\times(\frac{\lambda_g}{d_p}) \tag{14}$$

As stated in Yang et al. [28], the EMMS drag model is used to consider the influence of the sub-grid scale effect. Similarly, the sub-grid scale structure is also expected to influence the computed interphase heat transfer. According to our understanding of the sub-grid scale effect, the computed heat transfer coefficient between gas and particles is also expected to be higher than the actual heat transfer coefficient. However, Barracuda is not an open-source software, we could not incorporate the sub-grid scale effect in the heat transfer model now. We would recommend that the software vendor considers the effect of sub-grid scale structure on the interphase heat transfer in subsequent versions.

Based on the current fluidization knowledge, gas-particle heat transfer in a fluidized bed is very efficient due to the large heat transfer interface area provided by the small-diameter particles (particularly the smaller diameter Geldart A particles in this study) and the very strong solids convection due to bubble movement. It is widely accepted that the temperatures of gas and particles will approach to be equal very soon once gas is ejected into the bed. Therefore, the higher computed heat transfer coefficient due to the negligence of sub-grid scale structure is not expected to have strong influence on the simulation accuracy.

2.3. Coke burning kinetics model

In the MP-PIC model, the coke burning kinetics equations can be coupled in two ways, i.e., Volume Average Chemistry (VAC) and Discrete Particle Chemistry (DPC) methods. Both methods solve the chemical reactions using sub-time steps within each hydrodynamic time step. For VAC, the computational cell is regarded as the control volume of chemical reactions, and the calculated reaction rate is applied to the cell as a whole. While for DPC, the reaction control volume is each computational particle, plus some fraction of the gas volume of the cell. In this study, we selected the VAC method to calculate the chemical reactions in regenerator. The pitfall of DPC, according to Berrouk et al., [27] is that it is impractical to solve all reactions simultaneously. Hence, the reactions are treated sequentially and randomized in order to determine which reaction should be calculated first for each particle. On the contrary, all reactions can be solved simultaneously in VAC using the Ordinary Differential Equation (ODE) solver since they can be calculated over the entire cell.

The coke-burning kinetics model from Arbel et al. [31] was used in this simulation. It's an improved and updated model based on a more detailed kinetic description in the regenerator using the full range of published data both on FCC regenerator performance and kinetic rates. It not only describes the CO to CO_2 combustion kinetics completely, but also considers the influence of catalytic effect of CO promoters. Moreover, the model is applicable in both full- and partial-burn modes as well as the transition from one to the other. The main chemical reactions and reaction kinetics equations in the regenerator are listed in Table 1.

Table 1
Chemical reactions and reaction kinetics equations in the regenerator.

Chemical reaction	Stoichiometric equation	Reaction kinetics equation
Carbon combustion	$C+\frac{1}{2}O_2\xrightarrow{r_1}CO$	$r_1=(1-\theta_g)k_1\frac{C_{rgc}}{Mw_C}\rho_c P_{O_2}$
Carbon combustion	$C+O_2\xrightarrow{r_2}CO_2$	$r_2=(1-\theta_g)k_2\frac{C_{rgc}}{Mw_C}\rho_c P_{O_2}$
CO homogeneous combustion	$CO+\frac{1}{2}O_2\xrightarrow{r_{3hom}}CO_2$	$r_{3hom}=\theta_g k_{3hom}P_{O_2}P_{CO}$
CO heterogeneous combustion	$CO+\frac{1}{2}O_2\xrightarrow{r_{3het}}CO_2$	$r_{3het}=x_{pt}(1-\theta_g)k_{3het}\rho_c P_{O_2}P_{CO}$
Hydrogen combustion	$H+\frac{1}{4}O_2\xrightarrow{r_4}\frac{1}{2}H_2O$	$r_4=(1-\theta_g)k_4\frac{H_{rgc}}{Mw_H}\rho_H P_{O_2}$

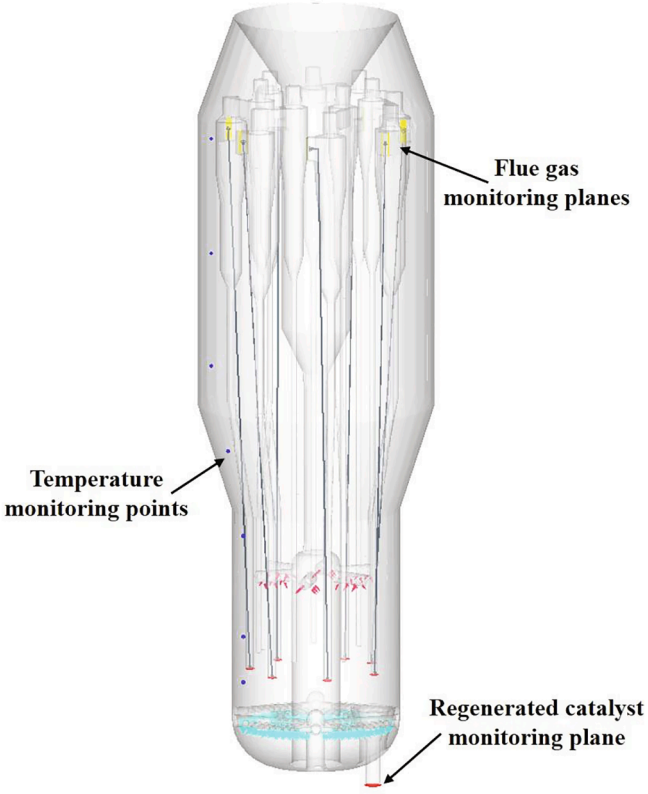

Fig. 1. Setup of the different monitoring points and monitoring planes.

The initial ratio of CO/ CO_2 at the catalyst surface, β_c, is obtained from Weisz [32], i.e.

$$\beta_c=\frac{k_1}{k_2}=\beta_{c0}\exp(\frac{E_\beta}{RT}) \tag{15}$$

$$k_c=k_1+k_2, k_1=\frac{\beta_c k_c}{\beta_c+1}, k_2=\frac{k_c}{\beta_c+1} \tag{16}$$

Here, β_{c0} is the pre-exponential constant, E_β is the activation energy, and k_c is the overall coke-burning rate coefficient. The values of the rate coefficients of all reactions can be found in Arbel et al. [31].

2.4. Other simulation setups

The geometric model of the industrial FCC regenerator, the mesh, the boundary conditions, the initial conditions, and the simulation parameter settings have been described in Part I of the two sequential papers

Table 2
Comparison between the simulated results and industrial data.

Items	Simulated results	Industrial data	Relative error
Temperature in the dense bed, K	949	955	−0.6%
Temperature in the upper freeboard, K	1022	1009	1.3%
Temperature in the middle freeboard, K	1003	981	2.2%
Temperature in the bottom freeboard, K	977	964	1.3%

[28]. However, to investigate the axial temperature profile in the regenerator and their change with time, a series of temperature monitoring points are set at different heights near the wall, as shown in Fig. 1. At the same time, the gas flow rate at the first-stage cyclone entrances of the seven pairs of two-stage cyclones is also monitored to investigate the change of concentration of each flue gas component with time. The carbon content and residence time of the regenerated catalyst are investigated by setting a monitoring surface at the outlet of the regenerated catalyst standpipe.

3. Results and discussion

3.1. Model validation

Table 2 shows the comparison between the simulation results and industrial data, which include the temperatures in the dense bed and the temperatures in the upper, middle and bottom regions of the freeboard. The simulation results are time-averaged from 350 s to 400 s. It can be seen that both the value and the trend of the simulation results are very close to and agreeable with the industrial data. The relative errors are all within a small range, thus further authenticating the accuracy of the MP-PIC model in simulating the gas-solids reactive flow system in this study.

3.2. Effects of spent catalyst distribution and Crosser grid on temperature profile

Fig. 2 gives the temperature change with time at different heights in the four different regenerators. It can be seen that, with the reactions going on, all the monitored temperatures become stabilize and fluctuate around specified constant values, especially when the simulation time is

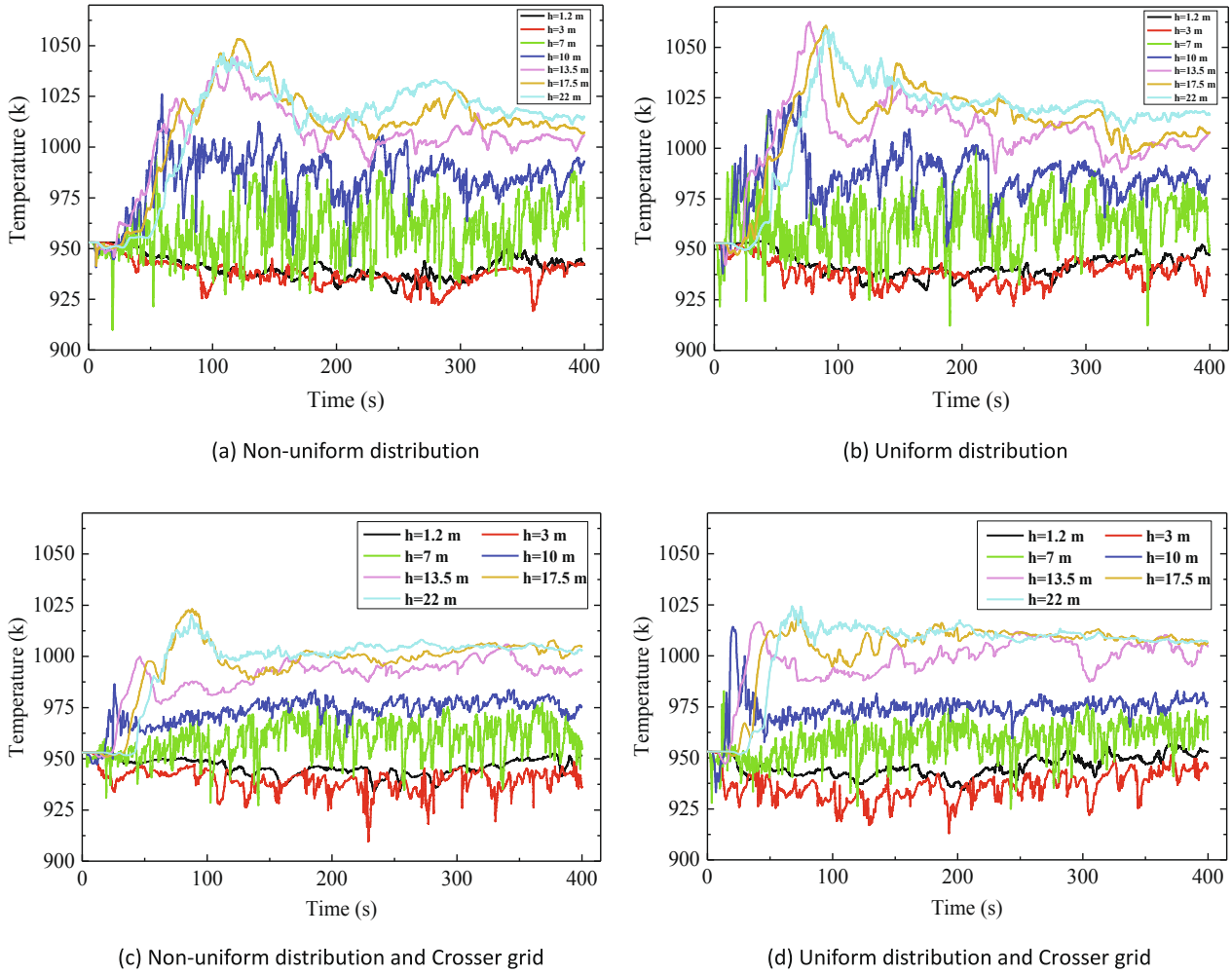

Fig. 2. Variations of temperature with time at different heights of the four different regenerators: (a) Non-uniform distribution; (b) Uniform distribution; (c) Non-uniform distribution and Crosser grid; (d) Uniform distribution and Crosser grid.

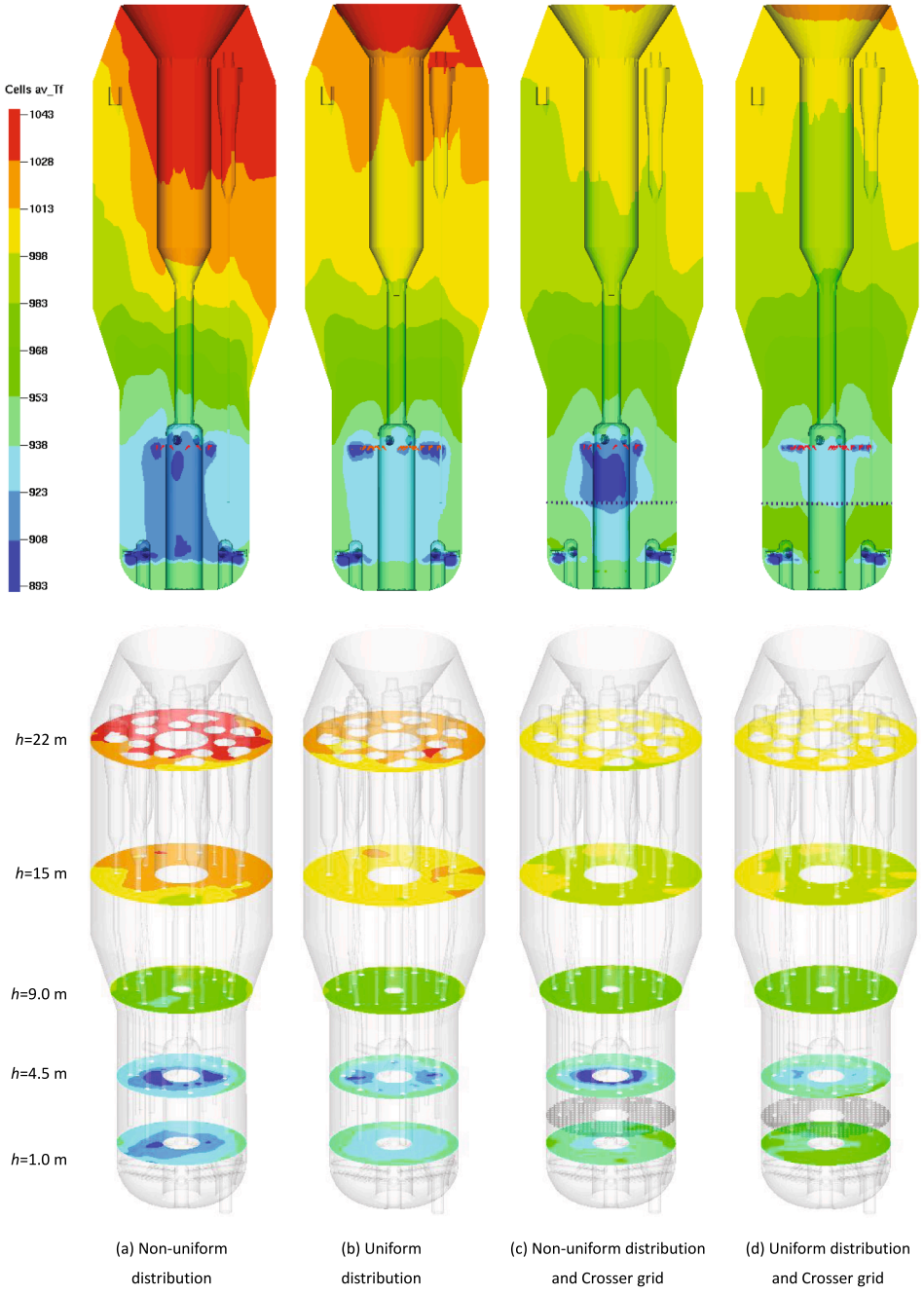

Fig. 3. Axial and radial contours of average temperature for four different regenerators: (a) Non-uniform distribution; (b) Uniform distribution; (c) Non-uniform distribution and Crosser grid; (d) Uniform distribution and Crosser grid.

greater than 350 s. The addition of Crosser grid has a significant improving effect on stabilizing the temperatures at different heights of the regenerator, as indicated by the smaller fluctuation magnitudes shown in Fig. 2(c) and (d). However, by comparing Fig. 2(a) and (b), it can be seen that the distribution uniformity of spent catalysts has a negligible temperature stabilization effect. For the two regenerators without Crosser grid, as shown in Fig. 2(a) and (b), the temperature fluctuation magnitudes are clearly higher than those in Fig. 2(c) and (d). The small temperature fluctuation magnitudes in the two regenerators with Crosser grid indicate better operating stability and should be related to the improved fluidization quality. In our previous large cold model experiment, [13] we have found that adding Crosser grid can sufficiently reduce the pressure fluctuation magnitude in the dense bed. We correlated this phenomenon to smaller bubble sizes and better gas-solids contact in the baffled fluidized bed. In Part I of the two sequential papers, [28] we have successfully demonstrated the predicted improvement on fluidization quality by the Crosser grid in the two baffled regenerators. Therefore, the predicted small temperature fluctuation magnitudes in the regenerators with Crosser grid are correlated to the improvement of fluidization quality. In addition, it is also found that the temperature at $h = 3$ m is slightly lower than that at $h = 1.2$ m and the fluctuation magnitude of the former is significantly greater than that of the latter. This is due to the influence of the continuous injection of cool spent catalysts and gas ($T = 673$ K) from the spent catalyst distributor at $h = 5.1$ m, which has a stronger influence on the bed temperature below and near it.

In order to investigate the influence of spent catalyst distribution and Crosser grid on the temperature profiles in the regenerator, both axial

and lateral distributions of the average temperature contours in the four different regenerators are compared, as shown in Fig. 3. It can be seen that, when using the non-uniform distribution form of spent catalyst, as shown in Fig. 3(a), an obvious low-temperature zone appears in the center zone below the spent catalyst distributor. This is mainly because there are only 12 injection points in this distributor and they are all arranged near the central roots of each distributor arm. Therefore, the low temperature spent catalysts entering the regenerator are more distributed in the center zone of the dense bed.

It is also found that a high-temperature zone appears in the upper zone of the freeboard. Moreover, the lateral temperature distribution in this zone is also very non-uniform. The reason for this phenomenon is that spent catalysts are not charged uniformly throughout the cross section of the regenerator, instead are agglomerated in the center zone of the dense bed. The result is that carbon is superfluous in some zones and O_2 is superfluous in the other zones. The two regenerators with non-uniform distribution of spent catalyst, i.e. Fig. 3(a) and (c), represent a bad matching between the distributions of spent catalyst and oxygen. However, the other two regenerators with uniform distribution of spent catalyst represent a good matching between the distributions of spent catalyst and oxygen. When the distributions of coke and O_2 is in bad matching, more CO is prone to be produced due to the partial burn mode, and is easier to escape into the freeboard. Otherwise, less CO is produced and is easier to be oxidized by O_2 to form CO_2. As unreacted CO and O_2 come into contact in the freeboard, fast combustion may be triggered. This is the so-call afterburning phenomenon. Since the catalyst inventory in the freeboard is small, the corresponding thermal capacity is low. The combustion of CO in the freeboard is easier to form a sharp rise in temperature. When afterburning is very serious, the excessive temperature rise may result in serious damage to the cyclone separators and other internal components. Unscheduled unit shutdown may have to start and serious economic loss is the result.

In industrial FCC regenerators, the degree of the seriousness of afterburning is usually judged by the temperature increase in the freeboard. It can be observed from Fig. 3(a) that there exists serious afterburning in the regenerator with non-uniform distribution of spent catalyst. The axial gradient of temperature in the freeboard is highest here. As the distribution of spent catalyst is improved, as the case shown in Fig. 3(b), the seriousness of afterburning is reduced as the observed axial gradient of temperature in the freeboard is decreased compared to Fig. 3(a). Moreover, the lateral temperature distribution uniformity is also improved. This is a result of better matching between the distributions of spent catalyst and oxygen due to the improvement in spent catalyst distribution uniformity.

After the Crosser grid is added, as shown in Fig. 3(c), the seriousness of afterburning in the freeboard is also reduced. The lateral temperature distribution is also more uniform compared to the case in Fig. 3(a). Comparing Fig. 3(b) and (c), it can be concluded that the effectiveness of adding Crosser grid to restrain afterburning is superior to improve the distribution of spent catalysts. Both the axial temperature gradient and the lateral temperature distribution uniformity in the freeboard (Fig. 3 (c)) is better than in Fig. 3(b). As suggested in Part I [28], the addition of Crosser grid can greatly improve the fluidization quality and gas-solids contact, which will accelerate the combustion CO in the dense bed, resulting in less CO escaping into the freeboard and less heat released due to the CO oxidation. With the addition of Crosser grid and improvement in spent catalyst distribution, i.e. the case in Fig. 3(d), the afterburning in the freeboard seems to be further restrained. However, there is little difference in the effect that can be observed comparing with Fig. 3(c) and (d).

Except for the axial temperature gradient and the lateral temperature distribution uniformity, the area of the low temperature zone (i.e. the area of the blue and light blue zones) in the dense bed can also be used to judge the performance of the regenerator. A thumb of rule is that the most serious afterburning in the freeboard usually corresponds to the largest area of low temperature zone in the dense bed. Compared with

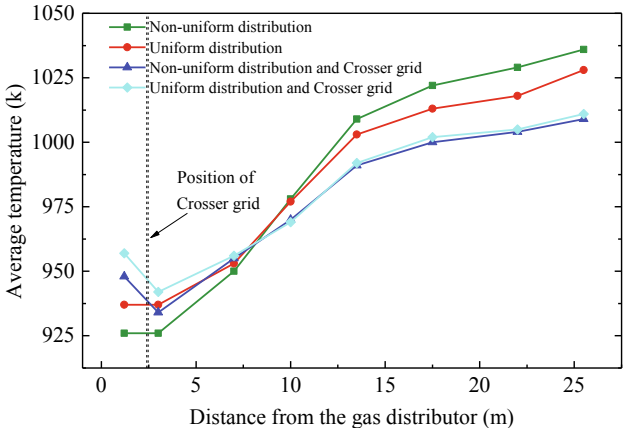

Fig. 4. Axial profiles of average temperature in the four different regenerators.

Fig. 3(a), both the addition of Crosser grid (Fig. 3(c)) and improvement in spent catalyst distribution (Fig. 3(b)) are all helpful in decreasing the area of the low temperature zone in the dense bed. Based on this criterion, the case in Fig. 3(d) is clearly the best as the area of the low temperature zone is the smallest.

In all the four subfigures of Fig. 3, we can see some areas of low temperature below the gas distributor in blue colors. These are the areas influenced by the interphase heat transfer, but the ratios of these influenced areas are very low. In other space (e. g. the major reaction volume above the distributor), the temperature distribution is dominated by the mixing of cold spent catalyst stream just entering into the bed and the hot catalyst already staying in bed for a long time. This agrees with the common understanding on gas-particle heat transfer in fluidized beds and verified our judgement of the negligible impact of interphase heat transfer.

Fig. 4 shows the variation of average temperature with axial height in the four different regenerators. It can be seen that, on the whole, the temperatures in all the four regenerators rise with the increasing axial height, but their increasing speeds, i.e. the axial temperature gradients, vary greatly. When there is no Crosser grid and spent catalyst distribution is not uniform, the temperature in the freeboard rises very rapidly with increasing height. The temperature difference between the freeboard and the dense bed is also the highest, indicating the most serious afterburning in the four regenerators. After the Crosser grid is added or spent catalyst distribution is improved, both the temperature and the temperature gradient in the freeboard clearly decreased. This demonstrates that the afterburning is restrained by the two measures. The temperature difference between the freeboard and the dense bed also decreases accordingly. Clearly, adding the Crosser grid is more effective than improving the spent catalyst distribution. When Crosser grid is added (Fig. 3(c), the temperature in the freeboard is lower than that without baffle (i.e. Fig. 3(a)). The maximum decrease is about 25 K. Comparatively, the maximum temperature decrease by the improvement of spent catalyst distribution is only about 10 K. When improved spent catalyst distribution joins with Crosser grid in the regenerator (i.e. Fig. 3(d)), There is little difference observed in Fig. 4 in view of the freeboard temperature. This is also consistent with the results shown in Fig. 3(c) and (d).

In addition, it is also found that, after the Crosser grid is added or the spent catalyst distribution is improved, the dense bed temperature increases accordingly. This is because as afterburning is restrained in the freeboard, more CO is combusted in the dense bed, resulting in higher heat release in the dense bed. It is observable in Fig. 4 that the increment of temperature in the dense bed is generally proportional to the decrement of temperature in the freeboard. As Crosser grid can restrain afterburning in the freeboard more effectively, the regenerators with Crosser grid have higher temperatures in the dense bed.

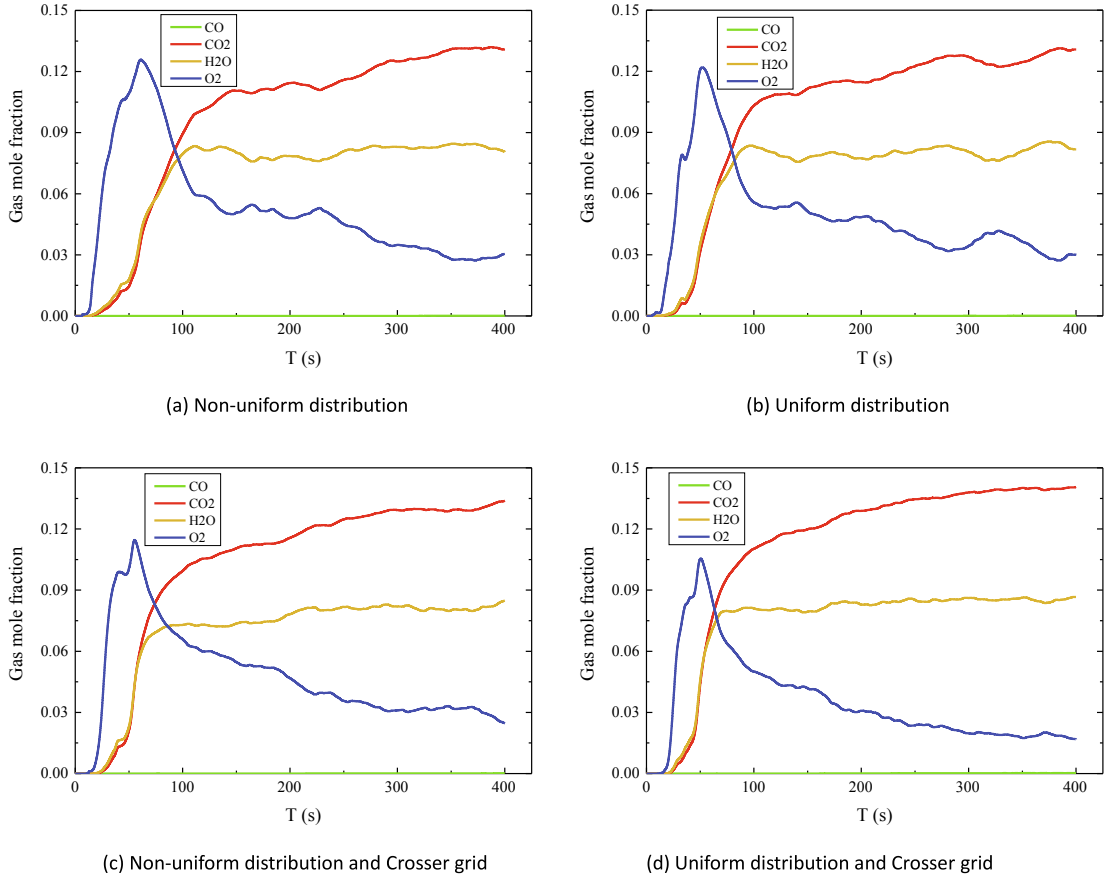

Fig. 5. Changes of fractions of main flue gas components with time in the four regenerators: (a) Non-uniform distribution; (b) Uniform distribution; (c) Non-uniform distribution and Crosser grid; (d) Uniform distribution and Crosser grid.

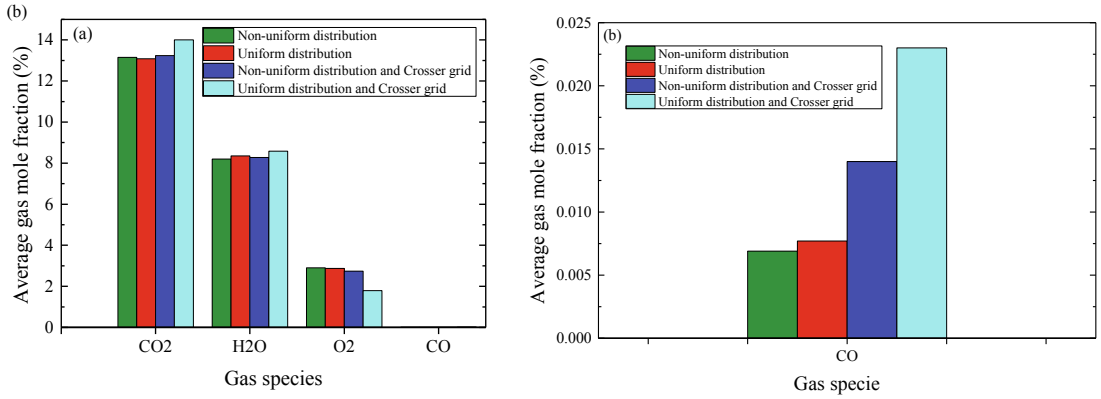

Fig. 6. Time-averaged fractions of main flue gas components at the outlets of the four regenerators (380 ~ 400 s).

Finally, it should be noted that the predicted temperature increment seems to be higher than that observed in industrial FCC regenerators, this should not be misconstrued for more serious afterburning. In our simulations, all the walls are treated as adiabatic walls, which neglects the heat loss that exists in actual FCC regenerators. Due to larger surface area and longer gas residence time in the freeboard sections, the heat loss can reduce the temperature in the freeboard to some extent.

3.3. Effects of spent catalyst distribution and Crosser grid on chemical reactions

Through the real-time monitoring of the gas at the entrances of the seven first-stage cyclones, the variations of flue gas components with simulation time in four different regenerators are obtained as shown in Fig. 5. It can be seen that, with the simulation progress, the fractions of main flue gas components gradually step into nearly stable levels. This trend can be clearly observed after $t > 350$ s. Although there still exist certain degrees of fluctuations for some components, this is mainly due to the dynamic adjustment of the regenerated catalyst outflow in order to ensure the stability of catalyst inventory in the regenerator. Moreover, the large volume and the high solids inventory of the regenerator also make it difficult to achieve a stabilization status in a short period.

In addition, the CO fractions in the flue gas of the four regenerators are all very low (close to 0), which indicates that the four regenerators

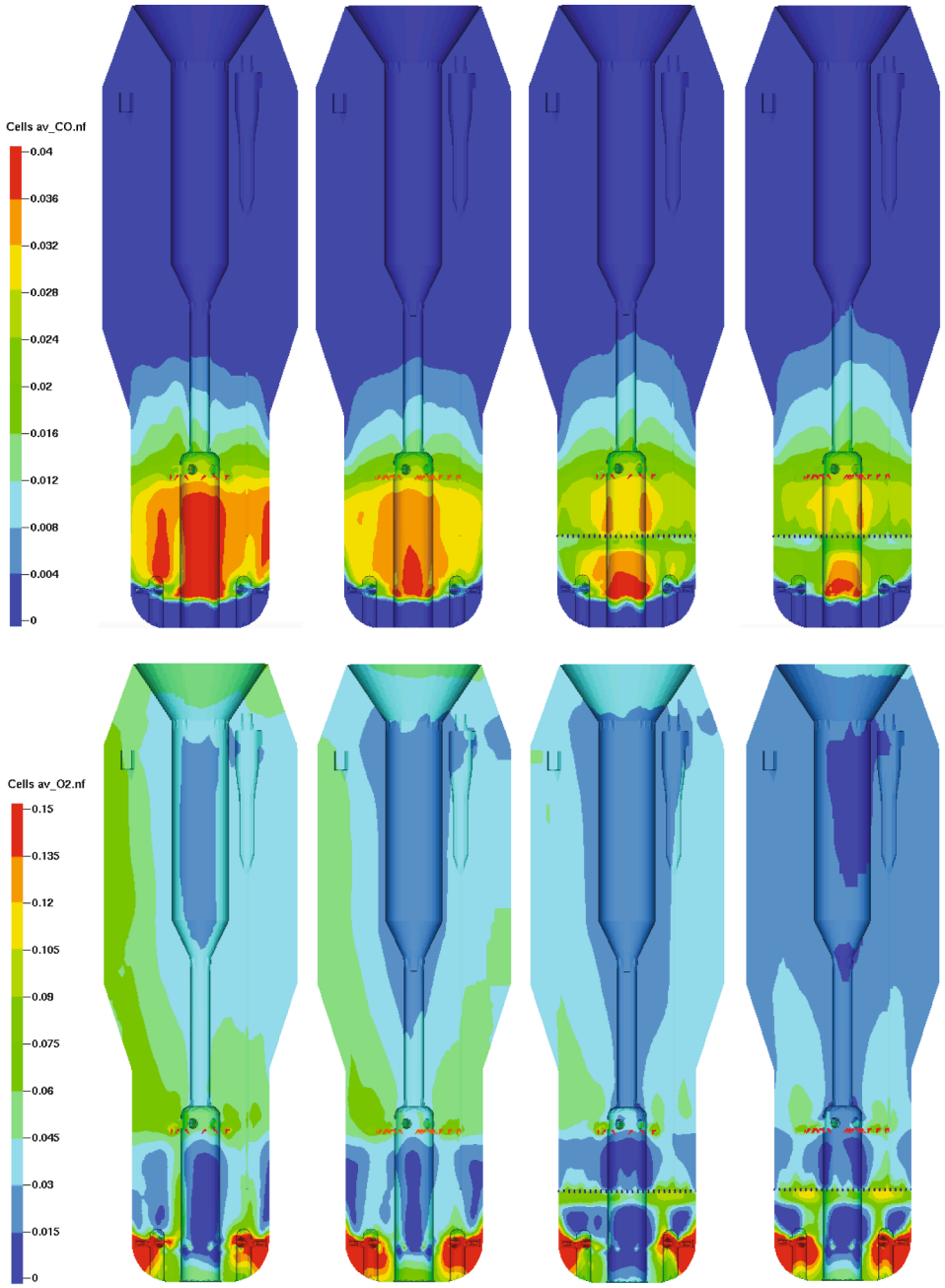

Fig. 7. Contours of average mole fractions of CO and O_2 in the four regenerators: (a) Non-uniform distribution; (b) Uniform distribution; (c) Non-uniform distribution and Crosser grid; (d) Uniform distribution and Crosser grid.

all belong to oxygen-enriched full-burn regeneration mode. Fig. 6 shows the time-averaged (380 ~ 400 s) mole fractions of the main flue gas components in the four regenerators. In general, the fractions of different flue gas components in the four regenerators are all close in values. The CO_2 concentration is the highest and the CO concentration is the lowest. However, for the regenerator with both uniform spent catalyst distribution and Crosser grid (i.e. the case shown in Fig. 3(d)), the fractions of CO_2 and H_2O are clearly higher than those in the other three regenerators. Accordingly, the O_2 fraction is significantly lower than that in the other three regenerators. Although the CO fractions in the flue gas outlet (Fig. 6(b)) are all very low, there are observable differences for the four regenerators. Compared with results shown in Figs. 3 and 4, the CO fraction here seems to be inversely proportional to the seriousness degree of freeboard afterburning.

Fig. 7 shows the contours of the average mole fractions of CO, O_2 and H_2O in the four regenerators. It can be seen that, when spent catalyst distribution is not uniform and no baffle is inserted in the dense bed, zones of extremely high fractions of CO and H_2O (red zones) and extremely low concentration of O_2 (blue zones) emerge in the central region of the dense bed, as shown in Fig. 7(a). The reason for this phenomenon has been described in Section 3.2. The spent catalysts enter from the root outlets of the distributor arms, resulting in a zone of very high carbon and hydrogen contents under the spent catalyst distributor. This triggers posthaste O_2 exhaustion in this zone. In turn, a large amount of CO is produced due to the partial combustion model of carbon in the catalyst. This is also a result of the bad matching between the

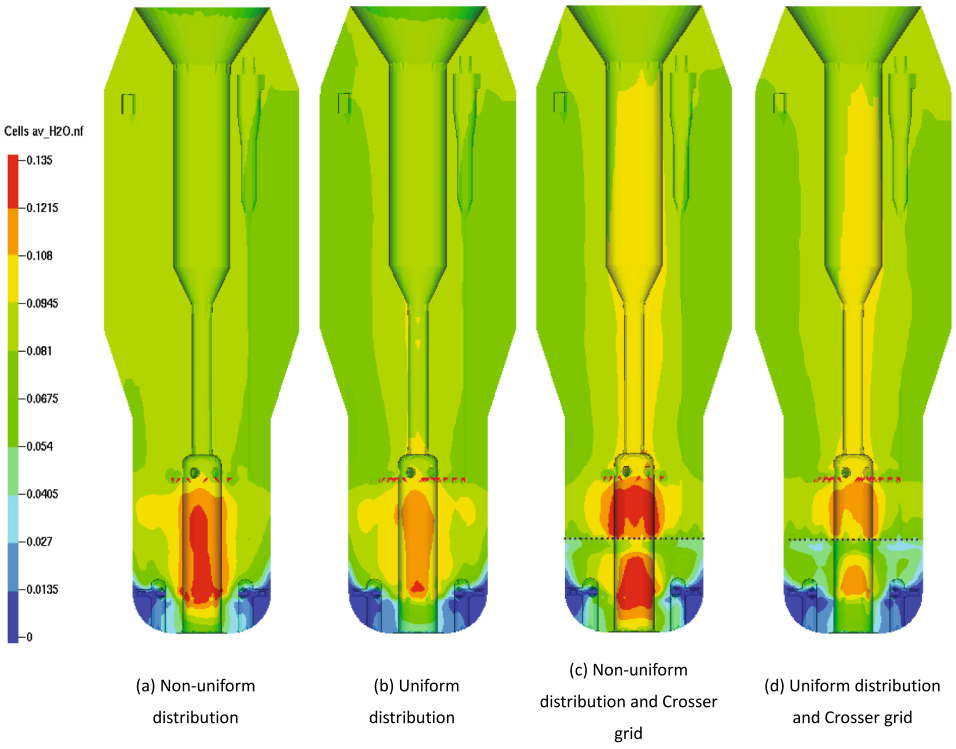

Fig. 7. (*continued*).

distributions of spent catalyst and oxygen and is closely linked with the most serious afterburning in the freeboard of this regenerator. It is also observed that the O_2 fraction distribution in the freeboard (Fig. 7(a)) is not very symmetrical and seems to be corresponding with the temperature distribution shown in Fig. 3(a). The region with low O_2 fraction in Fig. 7(a) seems to be corresponding with that in high temperature in Fig. 3(a). It is worth stating that the extremely high H_2O concentration in the axial region of the dense bed is a potential precursor to the hydrothermal inactivation of the catalyst in this region.

When spent catalyst distribution is improved, the distributions of CO, O_2 and H_2O fractions in the dense bed are also improved. Especially, the area of the zone with high CO and H_2O fractions decreases distinctly, as shown in Fig. 7(b). Similarly, when Crosser grid is added in the dense bed, the distributions of CO, O_2 and H_2O fractions in the dense bed improve further with an obvious decrease in the area of the zone with high CO fraction, as shown in Fig. 7(c). If spent catalyst distribution uniformity and Crosser grid function together, the effectiveness of improvement is the most remarkable as shown in Fig. 7(d). The distributions of CO and H_2O fractions become more uniform in the dense bed and the distribution of O_2 fraction becomes more symmetrical in the freeboard. These results are consistent to the predicted temperature results shown in Figs. 3 and 4. Meanwhile, the average fractions of CO and H_2O below the baffle are all lower than those above the baffle. The decrease of H_2O fraction throughout the dense bed also decreases accordingly, which is beneficial to protect the catalyst activity due to hydrothermal inactivation.

3.4. *Effects of spent catalyst distribution and Crosser grid on carbon content in catalyst*

The carbon content in regenerated catalyst is the most important and direct factor for accentuating the performance of regenerators since catalyst activity recovery is the primary objective of the FCC regenerator. Currently, the most widely utilized USY zeolite catalyst in FCC units usually demands the carbon content in regenerated catalyst to be lower than 0.05 ~ 0.1 w%. Therefore, the carbon content in regenerated catalyst is an indicator of the cleanness of the regenerated catalyst and the effectiveness of the regeneration performance.

Fig. 8(a) presents the change of the average carbon content in regenerated catalysts discharged from the standpipe outlet with the simulation time for the four regenerators. It can be seen that, for all the four regenerators, the average carbon content in regenerated catalysts show a similar trend with increasing simulation time, i.e. increasing rapidly and then decreasing slowly or fluctuating around a certain constant value. This is because the carbon content in catalysts in the initial condition ($t = 0$ s) is set to zero. The average carbon content in the regenerated catalyst starts from zero and increases with the continuous addition of spent catalyst with high carbon content. On the other hand, the coke combustion is another influencing factor that tends to decrease the carbon content in the regenerated catalyst. The change of carbon content in the regenerated catalyst reflects a competition between the two influencing factors. It can be seen from Fig. 8(a) that the importance of the latter becomes more and more important as the simulation time proceeds. There exists a critical transition time, after which it seems the two factors start to show comparative influences. Depending on the different coke-burning abilities, the transitional time seems to be different in the four regenerators.

In order to exclude the effect of the initial particles in the bed and reflect the regeneration performance more intuitively, Fig. 8(b) gives the change of the average carbon content of regenerated catalysts excluding the effect of the initial bed particles. In this simulation, the initial bed particles and the spent catalyst were set to be two types of solids. They have the same physical properties, such as particle size distributions, particle density, etc. The only difference between the two types of particle is the composition. There is a small fraction of coke in the spent catalysts which is treated as a combination of 98.839 wt% base catalyst, 1.057 wt% carbon, and 0.104 wt% hydrogen [28]. However, the composition of the initial bed particles is only 100 wt% base catalyst.

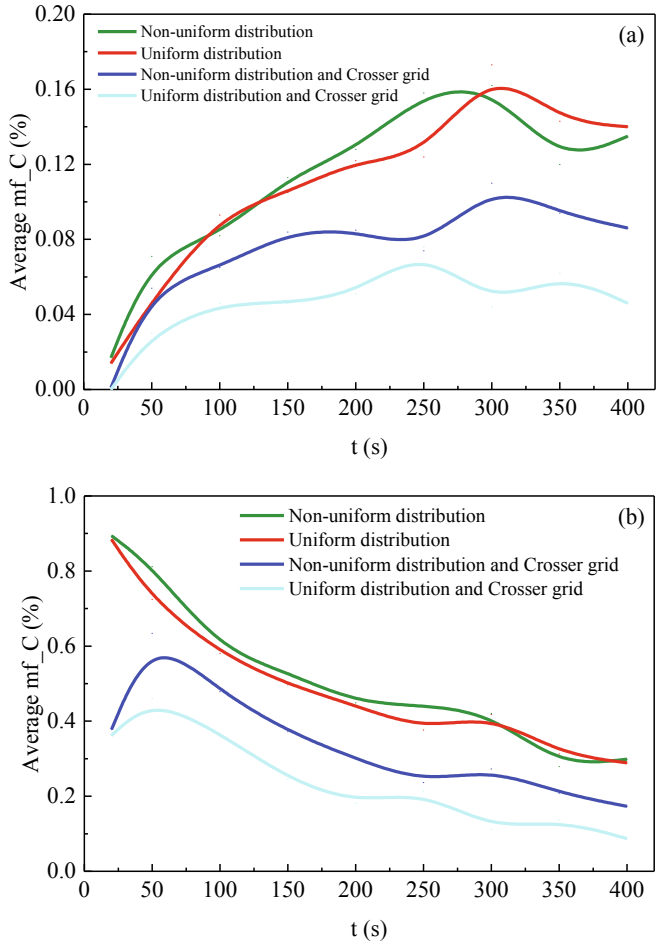

Fig. 8. Change of average carbon content in regenerated catalysts (a) and that excluding the influence of initial particles (b).

Therefore, to exclude the effect of the initial bed particles, only the spent catalysts are needed to calculate the carbon content in regenerated catalysts. It can be seen that the modified average carbon content in the regenerated catalysts first decreases sharply and then gradually in all the four regenerators. This is also a combined result of the two influencing factors, i.e. the continuous addition of spent catalyst and the coke combustion. It must be admitted that, even with near 7 min simulation time, none of the four regenerators is truly operated in a dynamically equilibrium status. According to the initial catalyst inventory and the macro catalyst circulation rate of this FCC unit, the average solids residence time in the regenerator is 562 s. It is well known that solids flow in a dense fluidized bed is approaching a typical CSTR pattern. It costs at least several times the average residence time to claim a full replacement of the initial particles in the bed. Therefore, the total simulation time in this study (400 s) is too short to replace all the initial particles in the bed and achieve a truly equilibrium operating status.

However, both Fig. 8(a) and (b) can be used to demonstrate the effectiveness of Crosser grid and spent catalyst distribution on improving the regenerator performance. In the two figures, it is seen that the two regenerators with Crosser grid both have significantly lower carbon contents in regenerated catalysts throughout the simulation period. The combination of improved spent catalyst distribution and Crosser grid can make the carbon content in regenerated catalysts the lowest in the four regenerators. Comparatively, when only spent catalyst distribution is improved, its improvement on catalyst regeneration is not very effective, as indicated by the small difference in carbon content in regenerated catalysts. However, with the help of Crosser grid, the effect of improved spent catalyst distribution can be much bigger, as indicated by the difference in carbon content in regenerated catalysts in the regenerator with Crosser grid (Fig. 3(c)) and that with both Crosser grid and improved spent catalyst distribution (Fig. 3(d)).

From Fig. 8(b), it can be seen that the modified carbon contents in regenerated catalysts in the two regenerators with Crosser grid are much lower than the carbon content in spent catalysts (1.057 wt%) in the early stage of simulation. However, they are very close to the carbon content in spent catalysts in the two regenerators without Crosser grid, this reflects the result of the strong suppression on axial solids backmixing by the Crosser grid. The detailed effect of Crosser grid on solids backmixing can be found in Part I of the two sequential papers [28]. In the early stage of simulation, only a small fraction of the newly added spent catalysts can enter into the lower part of the regenerator beneath the Crosser grid. The high O_2 partial pressure can make more coke in this part of spent catalyst exhausted. Moreover, the improved fluidization by the Crosser grid can further help to burn more coke. This can explain the much lower modified carbon contents in regenerated catalysts in the two regenerators with Crosser grid in the early stage of simulation.

Fig. 9 shows the axial and lateral contours of carbon content in catalysts in the four regenerators (at $t = 400$ s). It can be seen that, for the regenerator with non-uniform spent catalyst distribution (Fig. 9(a)), the carbon content of catalyst around the central spent catalyst standpipe is significantly higher than in other regions. More spent catalysts newly introduced into the dense bed are concentrated in the central region (red region). It is also found that some catalysts with very high carbon content have by-passed to the bottom regenerated catalyst standpipe. It is well believed that the strength of lateral solids mixing is at least an order lower than that of axial solids mixing in a fluidized bed [33]. For a large fluidized bed like the regenerator in this study, the axial solids mixing will be further enhanced, but the lateral solids mixing is comparatively much weaker. Therefore, a part of the spent catalyst will choose to move downward fast in the central region into the bed bottom. Unfortunately, this central region is in oxygen-depleted status as shown in Fig. 7(a). Therefore, more spent catalysts with high carbon content have the opportunity to by-pass into the regenerated catalyst standpipe. These account for the high carbon content in regenerated catalysts in this regenerator. In some industrial FCC units with inferior regeneration performance, a small part of black particles (also known as fish-eye) can be seen from the samples of regenerated catalyst. These black particles are actually the by-passed spent catalysts without enough burning on their deposited coke.

For the regenerator with uniform distribution of spent catalyst, as shown in Fig. 9(b), the carbon content distribution is significantly improved. A proof is the lateral contour of carbon content in the lowest monitored level of Fig. 9(b). The distribution of carbon content in this level is more homogeneous than that in Fig. 9(a). There is no region with very high carbon content (red region) in this level. As seen from the axial profile of carbon content of this regenerator, regions with very high carbon content (red region) are mostly concentrated in the upper zone of the dense bed. Only very few regions with very high carbon content (red region) in the lower zone of the dense bed and the regenerated catalyst standpipe are observed.

As the Crosser grid is installed, the regions with very high carbon content (red region) are limited in the upper zone of the dense bed above the Crosser grid. For the lower zone beneath the Crosser grid and the regenerated catalyst standpipe, regions with very high carbon content (red region) almost disappear. For the lateral contour of carbon content in the lowest monitored level of Fig. 9(c), the coke content is much lower and its distribution is also more homogeneous than that of Fig. 9(a). This reveals that the Crosser grid strongly suppresses axial solids backmixing. Particles with high carbon content are usually newly introduced spent catalysts whose residence times in the regenerator are still very short. As discussed in Part I of the two sequential papers [28], it is difficult for these particles to enter into the zone below the Crosser grid due to the strong suppression of solids mixing by the baffle. As there are few particles with short residence time in the zone below the Crosser grid, it is

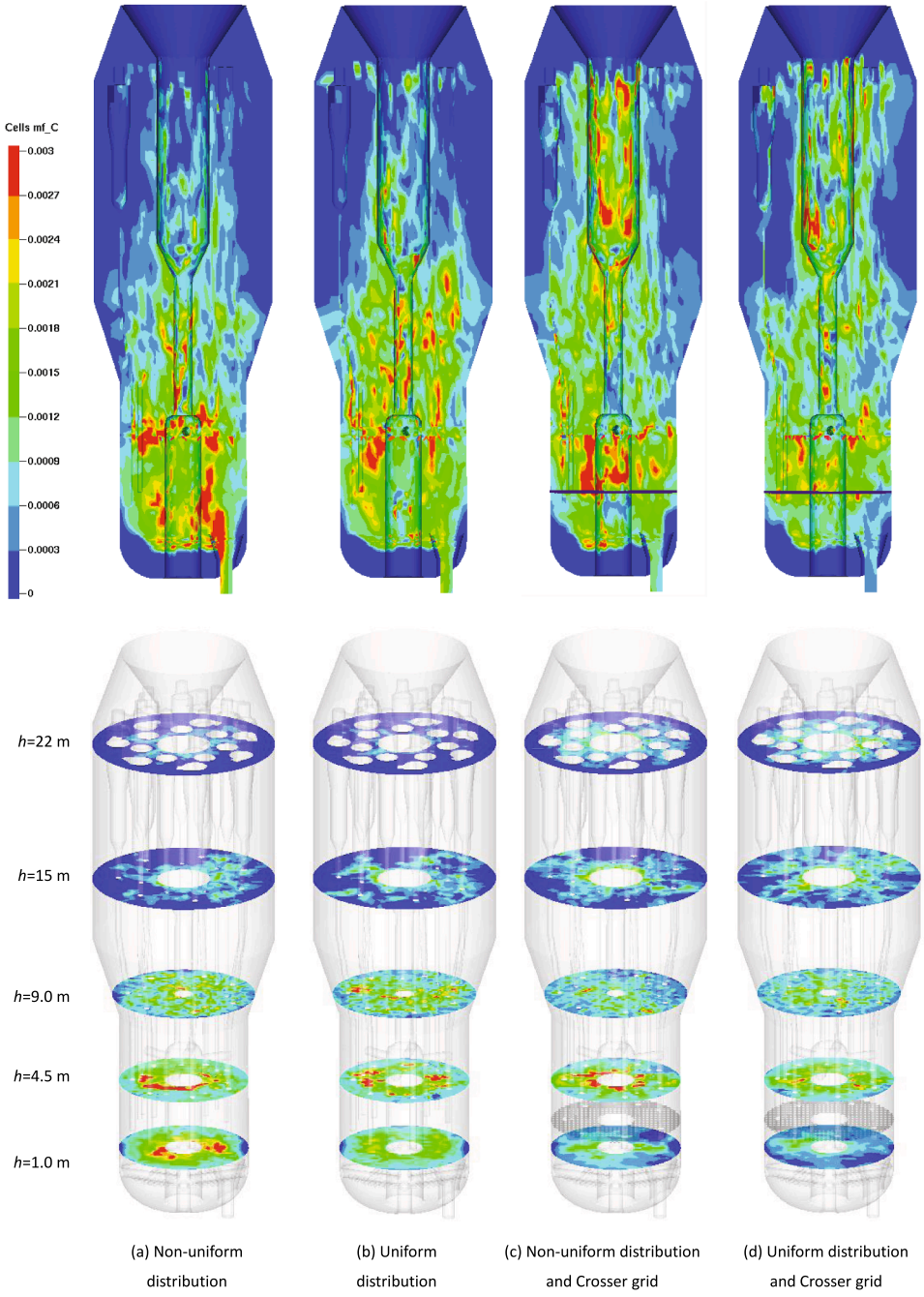

Fig. 9. Transient contours of mass fraction of carbon in catalysts in the four regenerators (t = 400 s): (a) Non-uniform distribution; (b) Uniform distribution; (c) Non-uniform distribution and Crosser grid; (d) Uniform distribution and Crosser grid.

easy to explain the lower carbon content in this zone.

When both improved spent catalyst distribution and Crosser grid are in combined action, both the axial and lateral distributions of carbon content are further improved as shown in Fig. 9(d). The uniform lateral spreading of spent catalysts increases their opportunity to contact with oxygen and to accelerate the combustion of coke. The Crosser grid helps restrain the by-passing of spent catalysts into the bottom zone and the regenerated catalyst standpipe. The results are that there are very few regions with very high carbon content (red region) throughout the regenerator. The carbon contents in the bottom zone below the Crosser grid and in the regenerated catalyst standpipe are further decreased.

The average carbon contents (380 ~ 400 s) in regenerated catalysts discharged from the bottom standpipe in the four different regenerators are calculated and shown in Fig. 10. Here, the carbon contents correspond to that shown in Fig. 8(a), i.e. the carbon content of the mixture of spent catalyst and the initial bed particles. It can be seen that when uniform distribution of spent catalyst and Crosser grid are both adopted, the average carbon content in regenerated catalysts is much lower than those of the other three regenerators. The decrease is about 61% compared with the original industrial regenerator without any intensification measure. Additionally, it is found that Crosser grid is more effective in reducing carbon content in regenerated catalysts than improving spent catalyst distribution.

Fig. 11 gives the statistics of residence time distribution of the catalysts discharged from the regenerated catalyst standpipe during 399 ~ 400 s in the four regenerators. Here, the residence time is the time of spent catalysts staying in the regenerator. As the discharge rate of the regenerated catalyst is about 177 kg/s, the sampling amount of catalyst

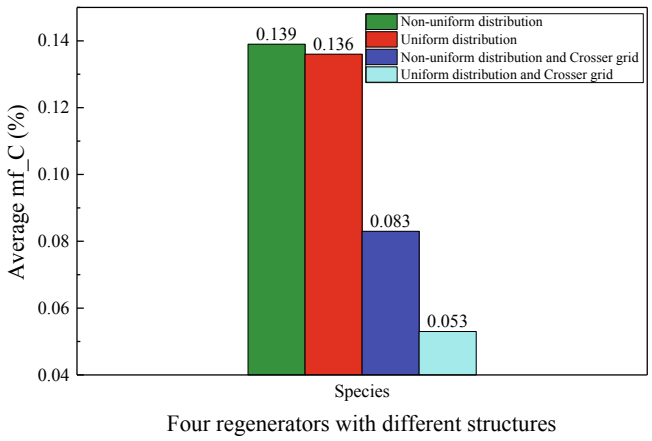

Fig. 10. Averaged mass fraction of carbon in regenerated catalysts (380 ~ 400 s).

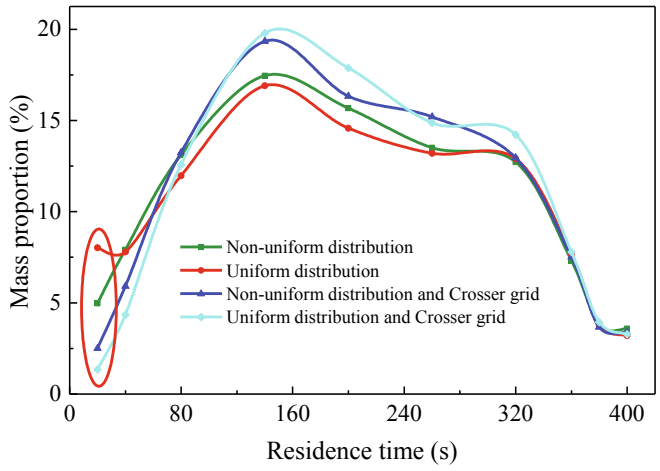

Fig. 11. Residence time distribution of the regenerated catalysts in the four regenerators.

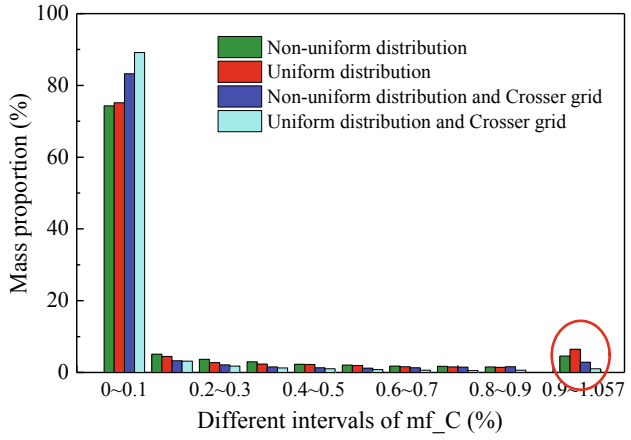

Fig. 12. Carbon content distribution of regenerated catalysts in the four regenerators.

in one second is large enough, which is far higher than the actual sampling amount during routine industrial operation. Meanwhile, the catalyst particles discharged from the regenerator in a short time interval for investigation is also more suitable to accurately analyze the solids residence time distribution. The distribution in Fig. 11 excludes the initial bed particles. The vertical coordinate represents the mass fraction of the spent catalysts with a certain residence time. It can be seen that the width of residence time distribution is the smallest and the peak value is the highest when uniform distribution of spent catalyst and Crosser grid are in combined action. Accordingly, the fraction of solids bypassing into the regenerated catalyst standpipe is smallest. In an FCC regenerator, narrow solids residence time distribution is helpful to improve its performance, especially in achieving lower carbon content in regenerated catalysts. An important reason to use two-stage regenerator design in some residue FCC units is due to the narrower solids residence time distribution, which can help to burn catalyst cleaner without increasing the regenerator geometry significantly.

Crosser grid is more effective in reducing the width of solids residence time distribution than improving spent catalyst distribution. This is mainly attributed to its strong suppression of axial solids back-mixing. In this aspect, it functions as a means to changing the previous single-stage regenerator into a pseudo-two-stage regenerator. An unexpected phenomenon is found as shown in Fig. 11, in the regenerator with the uniform distribution of spent catalyst, where the fraction of regenerated catalysts with residence time less than 20 s is much higher than that in the regenerator with the non-uniform distribution of spent catalyst. This indicates that more spent catalysts in this regenerator choose to by-pass into the regenerated catalyst standpipe with a very short time staying in the regenerator.

Fig. 12 shows the carbon content distribution of regenerated catalysts in the four regenerators. Here, the sampled particles are the regenerated catalysts discharged from the standpipe at 380 ~ 400 s and the vertical coordinate represents the mass fraction of catalysts with a certain carbon content interval. In general, most of the sampled regenerated catalysts in the four regenerators have carbon content less than 0.1 w%. Only a small fraction of catalysts have carbon contents greater than 0.1 w%. Compared with the other three regenerators, the regenerator with uniform distribution of spent catalyst and Crosser grid has the highest fraction (>90 w%) of regenerated catalysts with carbon content less than 0.1%. This is consistent with its lowest carbon content in regenerated catalysts (Fig. 10). For this carbon content interval, the regenerator without any intensification measure has the lowest fraction of regenerated catalysts. Comparatively, the Crosser grid is more effective to increase the fraction of regenerated catalysts in this carbon content interval.

However, an unexpected phenomenon also appears in the highest carbon content interval of 0.9 ~ 1.057 w%. This part of particles corresponds to the spent catalysts who choose to by-pass into the regenerated catalyst standpipe. For the two regenerators without Crosser grid, the fraction of this carbon content interval is obviously higher than other intervals except for carbon content interval of 0 ~ 0.1 w%. Among them, the regenerator with uniform distribution of spent catalyst has the highest fraction of catalyst of this carbon content interval. This agrees with the findings in Fig. 11 where the fraction of regenerated catalysts with residence time less than 20 s is the highest.

In view of the abnormal phenomena found in Figs. 11 and 12, the structure of the regenerator with uniform distribution of spent catalyst is examined and analyzed carefully. It is found that the possible reason for the above results is that, in one of the distributor arms, there are two injection points of spent catalysts just located above the regenerated catalyst standpipe entrance below as shown in Fig. 13(a). As lateral solids mixing is weak and axial mixing is strong in this large fluidized bed, the spent catalysts leaving from the two injection points are very possible to by-pass rapidly into the bottom regenerated catalyst standpipe and leave the regenerator. In order to verify the above judgment and solve the problem of spent catalysts by-passing, the two injection points are closed as shown in Fig. 13(b). All spent catalysts are charged into the regenerator from the remaining 34 injection points. The other boundary conditions and parameter settings remain unchanged and MP-PIC simulations were further carried out on this modified regenerator.

The same statistics and data processing methods are used for the

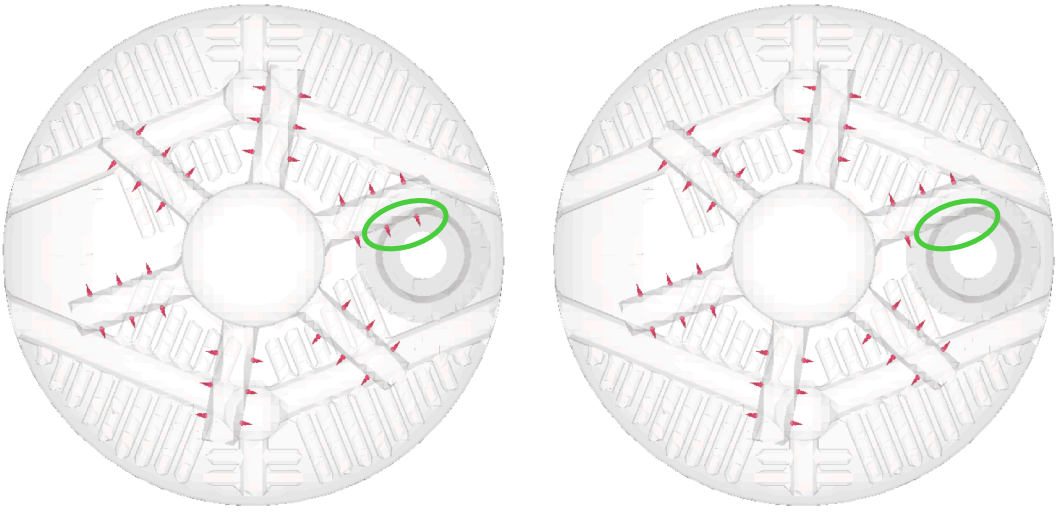

(a) Uniform distribution (b) Modified uniform distribution

Fig. 13. Top view of the uniform spent catalyst distributor before and after modification: (a) Uniform distribution; (b) Modified uniform distribution.

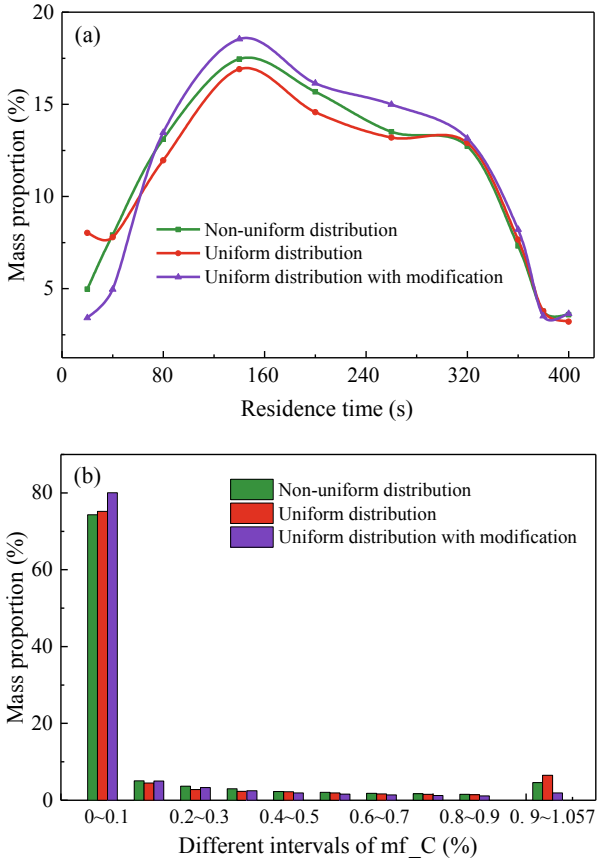

Fig. 14. Residence time distribution (a) and carbon content distribution (b) of regenerated catalysts.

simulation results of the modified regenerator. Its residence time distribution and carbon content distribution of the regenerated catalysts in this modified regenerator are shown in Fig. 14. To facilitate comparison, corresponding results of the two regenerators with uniform and non-uniform distributions of spent catalyst are also plotted in the two subfigures.

As can be seen from Fig. 14(a), after modification of the uniform spent catalyst distributor, the width of the residence time distribution curve becomes narrower, and the peak value increases. Meanwhile, the fraction of regenerated catalysts with residence time less than 20 s decreases significantly and is also smaller than that in the regenerator with non-uniform distribution of spent catalyst. It can also be seen from Fig. 14(b) that, after adopting the modified uniform spent catalyst distributor, the fraction of regenerated catalysts in carbon content of 0.9 ~ 1.057 w% is also reduced to a level smaller than that in the regenerator with non-uniform distribution of spent catalyst. Meanwhile, the fraction of regenerated catalysts with carbon content less than 0.1% also increases significantly and is higher than in the other two regenerators. Using the same data processing method as in Fig. 10, the average carbon content in regenerated catalysts is now 0.094% after adopting the modified uniform spent catalyst distributor, which is 31% lower than that before the modification. The above results suggest that the by-passing problem of spent catalysts is solved by a very simple modification and the performance of the regenerator is further improved. A guiding principle can hence be concluded in the design of a spent catalyst distributor for an industrial FCC regenerator. Except for pursuing uniformity in the cross section of the regenerator, spent catalyst outlets from the distributor should not be located in the area just above the bottom entrance of the regenerated catalyst standpipe, otherwise, some spent catalysts may choose to by-pass directly into the regenerated catalyst standpipe and leave the regenerator. Finally, it should be noted that, as the simulation accuracy of the MP-PIC method may not be high enough, more validation efforts are still needed to confirm the above conclusion in the future.

In summary, with the help of the MP-PIC simulation, the two intensification measures, i.e. adding horizontal baffle and improving spent catalyst distribution, have all proved their effectiveness in enhancing the performance of an industrial FCC regenerator. More flow-reaction coupling mechanisms are capable to be understood in more depth. The effectiveness of different intensification measures depends both on the resulted matching quality between the distributions of spent catalyst and oxygen in main air and the solids residence time distribution. Comparatively, adding a properly design horizontal baffle is proved to be more effective and should be the primary choice. With the help of horizontal baffles, installing a new distributor with improved spent catalyst distribution can further improve the performance. However, the above guiding principle should be taken in mind in properly arranging the outlets of spent catalysts in the distributor.

4. Conclusions

(1) With coupled coke-burning kinetics model, the MP-PIC simulation successfully predicts the temperature profile in an industrial regenerator, which is in good agreement with the industrial data.
(2) Adding a layer of Crosser grid in the dense bed can significantly reduce the temperature fluctuations, thus effectively improving the operating stability of the regenerator. Both improved spent catalyst uniformity and Crosser grid can restrain the afterburning in the freeboard as indicated by the decreased temperature difference between the dense bed and freeboard, the improved distributions of flue gas components, and the enhanced utilization efficiency of main air. Comparatively, the latter is more effective than the former.
(3) Both uniform spent catalyst distribution and Crosser grid can improve the distribution of spent catalysts, thus making better matching between the distributions of spent catalyst and oxygen in main air to realize more efficient coke burning and cleaner regenerated catalysts. However, Crosser grid is proved to be more effective than uniform spent catalyst distribution. The combination of the two intensification measures can help to achieve the most efficient coke burning and cleanest regenerated catalysts.
(4) After adding Crosser grid in the dense bed, the residence time distribution and carbon content distribution of regenerated catalysts are both narrowed and their peak values are both increased. A small structural modification was found to able to solve the spent catalyst by-passing problem existing in the regenerator with a uniform spent catalyst distributor, thus suggesting a guiding principle in designing industrial spent catalyst distributor.
(5) The MP-PIC simulation conducted in this study successfully proved the effectiveness of two intensification measures, i.e. adding horizontal baffle and improving spent catalyst distribution, in enhancing the performance of an industrial FCC regenerator. More flow-reaction coupling mechanisms are being understood in more depth by the simulation. The effectiveness of different intensification measures depends both on the resulted matching quality between the distributions of spent catalyst and oxygen in main air and the solids residence time distribution. Comparatively, adding a properly design horizontal baffle is proved to be more effective and should be the primary choice in industrial regenerators. Better spent catalyst distributor should be used with horizontal baffles to further improve its performance.

Declaration of Competing Interest

The authors declare that they have no known competing financial interests or personal relationships that could have appeared to influence the work reported in this paper.

Acknowledgments

The authors acknowledge financial support by the National Natural Science Foundation of China (21276273), the Science Foundation of China University of Petroleum, Beijing (2462015YQ0312 and C201606) and the National Key Research and Development Program (No. 2018YFF01011400).

References

[1] J. Chen, Catalytic Cracking Process and Engineering (2ED), China Petrochemical Press, Beijing, China, 2005 (in Chinese).
[2] B. Jiang, Study on installation of grids in turbulent-bed regenerator, Petrol. Refinery Eng. 40 (2010) 33–36 (in Chinese).
[3] Z. Shao, Foreign Refining and Petrochemical Technology Handbook, Chemical Industry Press, Beijing, China, 2004 (in Chinese).
[4] X. Liu, Research on the novel FCC regenerator with a post coke burning riser and its separator, Doctoral Dissertation, China University of Petroleum, Beijing, China, 2005 (in Chinese).
[5] G.J. Green, T. Yan, Fluidized bed combustion process and apparatus, US Patent, 4991521, 1991.
[6] J.R. Murphy, Catalyst regeneration process with improved catalyst distribution in a fluidized bed, US Patent, 4615992, 1986.
[7] R.B. Peterson, C. Santner, M. Tallman. Catalyst regenerator with a centerwell, US Patent, 7153479, 2006.
[8] Z. Zhang, Z. Bi, G. Tian, Regeneration equipment for fluidized catalytic cracking catalyst, China Patent, ZL 02139284, 2003 (in Chinese).
[9] R.B. Miller, T.X. Katy, Y. Yang, Staged catalyst regeneration in a baffled fluidized bed, US Patent, 6503460, 2003.
[10] R.B. Miller, E. Gbordzoe, Y. Yang, Solution for reducing NO_X and particulate emissions from FCC regenerators, NPRA, San Antonio, 2004.
[11] A.V. Sapre, T.M. Leib, D.H. Anderson, FCC regenerator flow model, Chem. Eng. Sci. 45 (1990) 2203–2209.
[12] C. Lu, Y. Zhang, A new internal for gas-solid fluidized beds, China Patent, ZL 10114153, 2006 (in Chinese).
[13] Y. Zhang, C. Lu, Experimental Study and modeling on effects of a new multilayer baffle in a turbulent fluid catalytic cracking regenerator, Ind. Eng. Chem. Res. 53 (5) (2014) 2062–2066, https://doi.org/10.1021/ie4025837.
[14] Y. Zhang, Q. Wang, The application of crosser grid in fluid catalytic cracking unit, Sino-Global Energy 15 (2010) 69–71 (in Chinese).
[15] X. Li, Y. Zhang, Q. Yu, Y. Zheng, R. Liu, C. Lu, Revamping for reinforced regeneration of a 500,000 TPY residue FCC Unit, Petrol. Refinery Eng. 43 (2013) 10–13 (in Chinese).
[16] Y. Xi, S. Zhou, C. Lu, Application of regeneration process optimization technology in FCC unit, China Powder Sci. Technol. 25 (2019) 39–44 (in Chinese).
[17] Y. Du, L. Zhang, A.S. Berrouk, Exergy analysis of propane dehydrogenation in fluidized bed reactor: experimental and MP-PIC Simulation, Energy Convers. Manage. 202 (2019), 112213.
[18] Y. Du, A.S. Berrouk, L. Sun, W. Sun, D. Fang, W. Ren, Experimental and CFD investigations of light alkane dehydrogenation in a fluidized bed reactor, Energy Fuels 33 (2019) 4177–4189.
[19] A.S. Berrouk, C. Pornsilph, S. Bale, Y. Du, K. Nandakumar, Simulation of a commercial FCC riser using a combination of MP-PIC and 4-lump oil-cracking kinetic models, Energy Fuels 31 (2017) 4758–4770.
[20] J. Wang, Continuum theory for dense gas-solid flow: a state-of-the-art review, Chem. Eng. Sci. 215 (2020) 115428, https://doi.org/10.1016/j.ces.2019.115428.
[21] J. Chang, J. Zhao, K. Zhang, J. Gao, Hydrodynamic modeling of an industrial turbulent fluidized bed reactor with FCC particles, Powder Technol. 304 (2016) 134–142, https://doi.org/10.1016/j.powtec.2016.04.048.
[22] B. Amblard, R. Singh, E. Gbordzoe, L. Raynal, CFD modeling of the coke combustion in an industrial FCC regenerator, Chem. Eng. Sci. 170 (2017) 731–742, https://doi.org/10.1016/j.ces.2016.12.055.
[23] G. Tang, A. Silaen, B. Wu, D. Fu, D. Agnello-Dean, J. Wilson, Q. Meng, S. Khanna, C.Q. Zhou, Numerical study of a fluid catalytic cracking regenerator hydrodynamics, Powder Technol. 305 (2017) 662–672, https://doi.org/10.1016/j.powtec.2016.09.082.
[24] G. Tang, A.K. Silaen, B. Wu, D. Fu, D. Agnello-Dean, J. Wilson, Q. Meng, S. Khanna, C.Q. Zhou, Numerical simulation and optimization of an industrial fluid catalytic cracking regenerator, Appl. Therm. Eng. 112 (2017) 750–760, https://doi.org/10.1016/j.applthermaleng.2016.10.060.
[25] J. Chang, G. Wang, X. Lan, J. Gao, K. Zhang, Computational investigation of a turbulent fluidized-bed FCC regenerator, Ind. Eng. Chem. Res. 52 (11) (2013) 4000–4010, https://doi.org/10.1021/ie3013659.
[26] R. Singh, E. Gbordzoe, Modeling FCC spent catalyst regeneration with computational fluid dynamics, Powder Technol. 316 (2017) 560–568, https://doi.org/10.1016/j.powtec.2016.10.058.
[27] A.S. Berrouk, A. Huang, S. Bale, P. Thampi, K. Nandakumar, Numerical simulation of a commercial FCC regenerator using Multiphase Particle-in-Cell methodology (MP-PIC), Adv. Powder Technol. 28 (11) (2017) 2947–2960, https://doi.org/10.1016/j.apt.2017.09.002.
[28] Z. Yang, Y. Zhang, A. Oloruntoba, J. Yue, MP-PIC simulation of the effects of spent catalyst distribution and horizontal baffle in an industrial FCC regenerator. Part I: Effects on hydrodynamics, Chem. Eng. J. 412 (2021), 128634.
[29] P.J. O'Rourke, Collective drop effects on vaporizing liquid sprays, Technical report submitted to the U.S. Department of Energy by Los Alamos National Laboratory., NM (USA), 1981 321–325.
[30] D.M. Snider, S.M. Clark, P.J. O'Rourke, Eulerian–Lagrangian method for three-dimensional thermal reacting flow with application to coal gasifiers, Chem. Eng. Sci. 66 (6) (2011) 1285–1295, https://doi.org/10.1016/j.ces.2010.12.042.
[31] A. Arbel, Z. Huang, I.H. Rinard, R. Shinnar, A.V. Sapre, Dynamic and control of fluidized catalytic crackers. 1. Modeling of the current generation of FCC's, Ind. Eng. Chem. Res. 34 (4) (1995) 1228–1243, https://doi.org/10.1021/ie00043a027.
[32] P.B. Weisz, Combustion of carbonaceous deposits within porous catalyst particles: III. The CO_2/CO product ratio, J. Catal. 6 (1966) 425–430.
[33] D. Kunii, O. Levenspiel, Fluidization Engineering, second ed., Butterworth-Heinmann, Boston, USA, 1991.